Nanotopography-controlled Cell Life and Death

G.Steven Huang and Chia-Wei Su

National Chiao Tung University, Institue of Nanotechnology, Hsinchu, Taiwan, ROC,
gstevehuang@mail.nctu.edu.tw

ABSTRACT

NIH-3T3 cells were grown on nanodot arrays to investigate how cells respond to nanolandscape. The nanodot arrays consisted nanodot of diameters ranging from 10 to 200 nm which were fabricated by AAO processing on Ta-coated wafers. Cells seeded on flat wafer surface and on 10 nm nanodot array appeared normal growth. Abnormal morphology occurred to cells cultured on arrays with dot size larger than 50 nm. The abnormality turned out to be apoptosis which was validated by casepase activity assay. Coating coating of fibronectin or type I collagen rescued the nanotopography-induced programmed cell death. Supplementation of cytochalasin D, an IP3-K inhibitor, to cells grown on 100 nm arrays triggered early apoptosis but did not enhance proportion of cells undergoing programmed cell death. This result indicated that nanotopography-induced apoptosis shared IP3 kinase pathway. Nanotopograpgy controls life and death of cells..

Keywords: NIH-3T3 cells, apoptosis, nanotopography, ECM

1 INTRODUCTION

The topology and chemistry of a surface contains information that directs cell behavior [1-5]. Cells interact with scaffoldings known as the extracellular matrix (ECM). The ECM consists of collagen and elastin fibers in 10–300 nm diameters which are intertwined into nanolandscape of peaks, valleys, and pores [6]. Cells detect and respond to specific ligands and spatial organization of the ECM. In addition to surface chemistry, the structure and topology of the matrix encodes important regulatory information for cells. Topography closely associates with cell adhesion, morphology, and cytoskeletal reorganization. Nevertheless, regarding topological constraints there is uncertainty using one dimensional structure such as fiber, ridge, or groove to probe cellular response. Such structures contain complex spatial information. The diameter may be 100 nm while the length can easily be tens of microns. Although fibrous structure of 100 nm in diameter stimulates proliferation, it is still not clear whether a topology consisting of hills of 100 nm in diameter promotes cell growth. Two-dimensional nanostructure was fabricated through varying the polymer blend and allowing spontaneous demixing [7]. The result is a nanotopography consisting of nanoscale islands with controllable heights of tens to hundreds of nanometers, with a large variation in diameter. It has been observed that 13-nm-high islands induce cell spreading and proliferation, while 160-nm islands retard attachment of filopodia. The large variation in diameter of the nanoscale islands introduces uncertainties to explore the size-dependent cellular response. A controlled 2D surface is required to better define the topological constraints that cells might respond to.

A matrix of nanodots with defined diameter and depth was fabricated by using aluminum nanopores as a template during oxidation of tantalum thin film [8]. The pore size of aluminum oxide is controllable and uniformly distributed; thus, it can serve as a convenient mold to fabricate tantalum into nanodot array of defined diameter. The 2D structure containing nanodots of uniform size will serve as a defined nanolandscape to investigate cellular response to topological variation.

2 MATERIALS AND METHODS

TaN thin film of 150 nm in thickness was deposited onto a 6-inch silicon wafer followed by deposition of 3 μm-thick aluminum on the top of a TaN layer. Anodization was carried out in 1.8 M sulfuric acid at 5 Volts for 10 nm nanodot array, or in 0.3 M oxalic acid at 25 Volts, 60 Volts, and 100 Volts for 50 nm, 100 nm, and 200 nm nanodot arrays, respectively. Porous anodic alumina was formed during the anodic oxidation. The porous alumina was removed by immersing in 5 % (w/v) H_3PO_4. A thin layer of platinum (ca 5 nm) was sputtered onto the structure to improve biocompatibility. The dimension and homogeneity of nanodot arrays were measured and calculated from images taken by JEOL JSM-6500 TFE-SEM and by atomic force microscopy (AFM). Coating of BSA, FN, and type I collagen was performed by covering nanodot arrays with 0.1 mg/mL protein solution at 4 ºC for 8 hr followed by rinsing with PBS three times before use. NIH-3T3 cells were cultured in Dulbecco's Modified Eagle's Medium complimented with 10% FBS and 5% CO_2 and incubated at 37 ºC in a class-10 clean room. The harvested cells were fixed with 1% glutaraldehyde , followed by post-fixation in 1% osmium tetroxide. Dehydration was performed through a series of ethanol concentrations and air dried. The specimen was sputter-coated with platinum and examined by JEOL JSM-6500 TFE-SEM at an accelerating voltage of 10 keV. EnzChek Caspase-3 Assay Kit #2 (Invitrogen, USA) was applied to evaluate caspase-3 activity following the procedure provided by the manufacturer.

3 RESULT AND DISCUSSION

3.1 The nanotopography

Scanning electron microscopy (SEM) and AFM images of nanodot arrays showed diameter/height of 15.3 ± 2.8 nm/11.3 ± 2.5 nm, 58.1 ± 5.6 nm/51.3 ± 5.5 nm, 95.4 ± 9.2 nm/101.1 ±8.3 nm, and 211.5 ± 30.6 nm/154.2 ± 27.8 nm for 10-nm, 50-nm, 100-nm, and 200-nm nanodot arrays, respectively (Fig 1). Dimensions of nanodots were well-controlled and highly defined.

3.2 Cellular response to nanodot arrays

NIH-3T3 cells were cultured on fabricated nanodot arrays and on flat wafer at the density of 1,000 to 5,000 cells per square centimeter. Cells were harvested at 24 hr, 48 hr, 72 hr, and 96 hr after seeding. SEM was performed to examine the morphology of cells (Fig 2). The side-view of SEM images provided alternative angles to evaluate the morphological change of cultured cells. Cells grown on control surface and 10-nm nanodot array remained flat and extended throughout the course of incubation. Cells grown on 50-nm nanodot array began to show an abnormal appearance on day 4. The abnormal cells underwent transformation of main cell body into subcellular spheres of ca 5 microns in diameter. On day 4, spherical sub-cellular cell bodies were visible. For cells grown on 100-nm nanodot array, comparable morphology occurred earlier from day 3; while for 200-nm nanodot array, morphological aberration started from day 2. The proportion of cells undergoing morphological change was higher and the event was triggered earlier on 100- and 200-nm nanodot arrays (Fig 3A).

The morphology of abnormal cells resembled cells proceeding programmed cell death. The occurrence of apoptosis was validated by caspase-3 activity assay performed on cells seeded on nanodot arrays following the time course (Fig 3B). The onset, time-dependent accumulation, and size-dependent profile of caspase-3 activity matched the proportion of cells undergoing morphological transformation on nanodot arrays. Nanotopography triggered apoptosis for cultured cells in a size-dependent and time-dependent manner. Arrays with dot-size larger than 50 nm triggered apoptosis.

3.3 Nanotopography affected formation of filopodia

Formation of focal adhesions reflected by the attachment of filopodia to the substratum indicates normal growth for cultured cells [9]. The number of filopodia extended from cells decreased for cells grown on nanodot arrays larger than 50 nm (Fig 4). For cells seeded on 200-nm nanodot array, very few filopodia were found. Cells grown on larger-sized nanodot arrays seemed to loose the ability to establish filopodia attachment.

3.4 Ligand binding but not hydrophobicity prevented nanotopography-induced apoptosis.

Topology and surface chemistry might share a common pathway to direct cell behavior. Focal adhesions are mediated by cell attachment through receptor-ligand binding [10-13]. The inability of cells to establish filopodia attachment on nanolandscape might be prevented by surface modification of ligands. We coated 100-nm nanodot array with BSA, FN, or type I collagen. Cells were seeded onto the pre-coated substrates (Fig 5). Pre-treatment of BSA did not prevent apoptosis while FN and collagen I coating completely averted apoptosis. FN and collagen are native substrates of integrins, the key transmembrane proteins of focal adhesions. Prevention of programmed cell death by the FN- or type I collagen-enforced cell anchorage indicated that topography-induced apoptosis could be overridden by receptor-mediated cell attachment.

To explore the possibility that surface hydrophobicity might play a role in the nanotopography-induced apoptotic event, the contact angles of nanodot arrays were measured (Fig 6). Contact angle increased while the sizes of nanodot arrays increased indicating that surface hydrophobicity increased with dot size. However, coating with BSA essentially eliminated the difference in contact angle. Since the BSA-coating did not prevent apoptosis, factors other than surface hydrophobicity were involved to determine cell fate when culturing on nanodot arrays.

3.5 Nanotopography-induced apoptosis was associated with IP-3K dependent pathway

Nanodot arrays triggered apoptotic pathways which might be shared by integrins-mediated formation of focal adhesions that lead to rearrangement of cytoskeleton [11, 12]. Cytochalasin D is a cell-permeable fungal toxin which binds to the barbed end of actin filaments inhibiting both the association and dissociation of subunits [14]. This causes the disruption of actin filaments and inhibition of actin polymerization. Cytochalasin D alone induces a dose-dependent cytoskeletal collapse that causes apoptosis [9, 15-17]. Cytochalasin D triggered apoptosis for cells cultured on control surface (Fig 7). For cells seeded on 100-nm nanodot array, administration of cytochalasin D triggered early onset of apoptosis. However, the accumulation rate of apoptosis remained essentially unchanged compared to untreated cells. The result indicated that the nanotopography induced apoptosis through PI-3K pathway [15, 16].

The current study provides evidence that topology is a key factor controlling cell behavior. The topological perception might share a common sensing and transmitting apparatus with integrins-mediated focal adhesions.

The current report is consistent with the results from nanoislands that 160-nm-deep nanoislands retard attachment of filopodia [7]. However, we did not observe

nanotopography-induced cell proliferation on nanodot arrays. The difference might be due to the geometric heterogeneity in diameter of nanoislands such that the various features of topology somehow confused the cells.

When grown on microscale ridges and grooves, cells are aligned in the direction of the grooves [4, 5]. It is likely that cells avoid growth across ridges or grooves to prevent apoptosis. Longitudinal growth is allowed and thus proliferated. However, the current study is insufficient to explain the proliferation of cells on nanotopography fabricated by random deposition of 100-nm nanofibers on glass slide. Further study with a defined fibrous-like surface consisting of various lengths and diameters of nanorods is likely to clarify the proliferation-topography relationship of a fibrous landscape.

4 ACKNOWLEDGMENTS

This study was supported in part by National Science Council Grant NSC94-2320-B-009-003 and Bureau of Animal and Plant Health Inspection and Quarantine Council of Agriculture Grants 95AS-13.3.1-BQ-B1 and 95AS-13.3.1-BQ-B6.

Figure 1

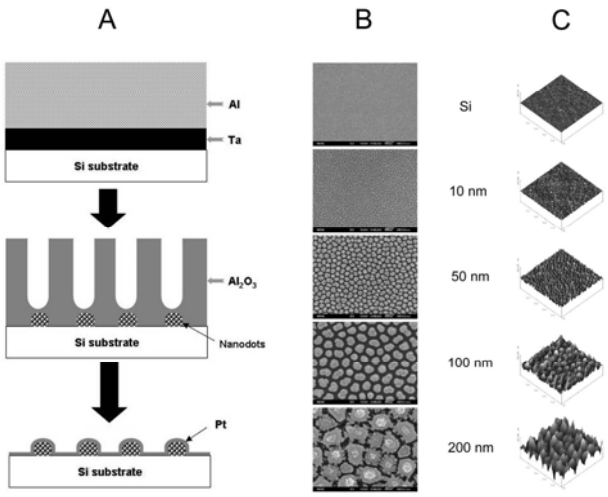

Fig 1. Fabrication of tantalum-based nanodot arrays using AAO processing. (A) Schematic representation of fabrication procedure. (B) SEM images of the fabricated nanodot arrays. (C) AFM images of the fabricated nanodot arrays. Images are arranged from left to right: unprocessed silicon (Si), 10-nm nanodot array (10 nm), 50-nm nanodot array (50 nm), 100-nm nanodot array (100 nm), and 200-nm nanodot array (200 nm).

Figure 2

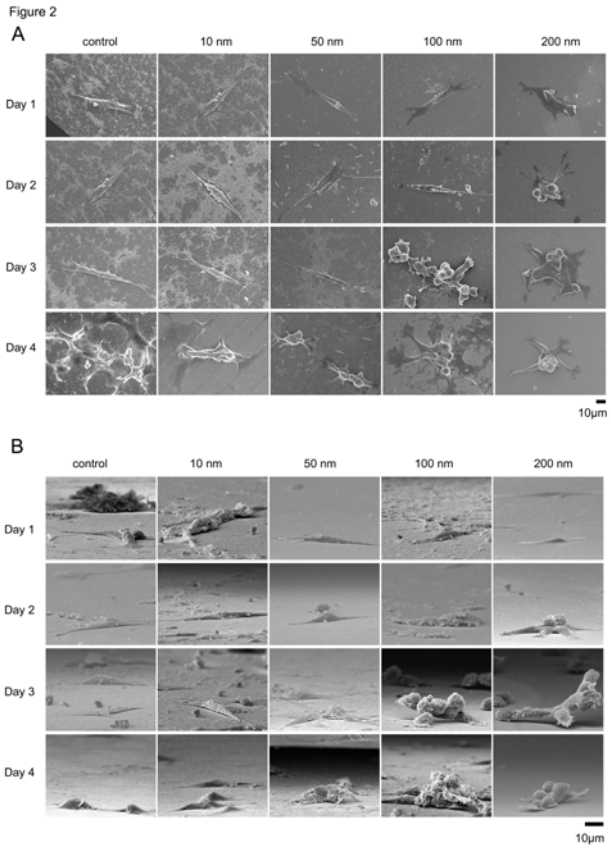

Fig 2. SEM images of cells seeded on nanodot arrays. NIH-3T3 cells were seeded on flat silicon surface, 10-nm nanodot array (10 nm), 50-nm nanodot array (50 nm), 100-nm nanodot array (100 nm), and 200-nm nanodot array (200 nm). The cells were harvested at 24 hr (Day 1), 48 hr (Day 2), 72 hr (Day 3), and 96 hr (Day 4) after seeding. SEM images were taken. Representative images are shown: (A) top view, (B) side view.

Figure 3

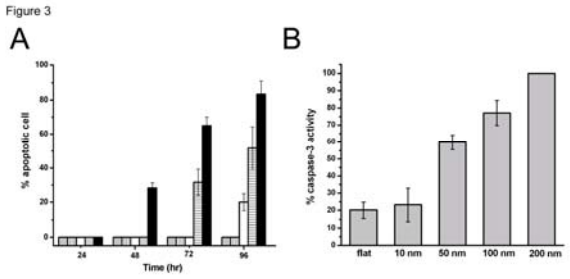

Fig 3. Apoptosis occurred to cells cultured on nanodot array. (A) Percentage of cells with abnormal morphology calculated from SEM images. Bars depict percent apoptotic cells grown on flat silicon surface (grey), 10-nm nanodot array (vertical line), 50-nm nanodot array (empty), 100-nm

nanodot array (horizontal line), and 200-nm nanodot array (filled). (B) Caspase-3 activity for cells cultured 96 hrs on nanodot arrays. Values were averaged from 6 sets of independent experiments and were expressed as mean value ± standard deviation.

Figure 4

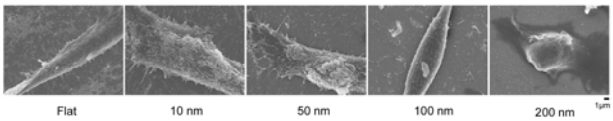

Fig 4. SEM images of NIH-3T3 cells cultured on nanodot arrays to show filopodia extended from cells.

Figure 5

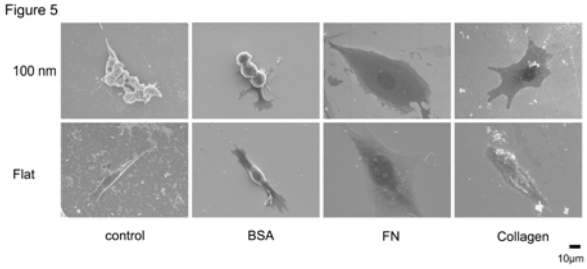

Fig 5. Effects of BSA-, FN-, and type I collagen- coating on the nanotopography-induced apoptosis. Cells were seeded on nanodot arrays and cultured for 96 hrs before harvest.

Figure 6

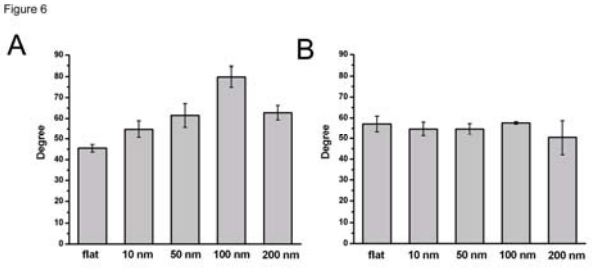

Fig 6. Contact angle measurements for the nanodot arrays. Contact angles were measured for untreated nanodot arrays (A) and BSA-treated nanodot arrays (B).

Figure 7

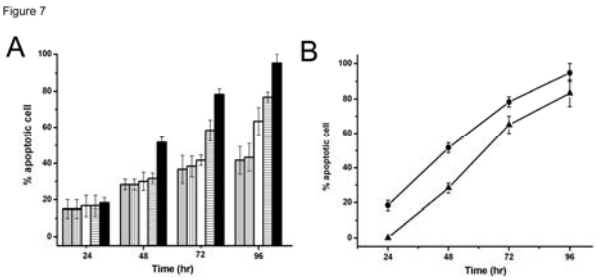

Fig 7. Effects of cytochalasin D to nanotopography-induced apoptosis. Cells were cultured on nanodot array for the designated time and morphologically aberrant cells were counted. (A) Bars depict percent apoptotic cells grown on flat silicon surface (grey), 10-nm nanodot array (vertical line), 50-nm nanodot array (empty), 100-nm nanodot array (horizontal line), and 200-nm nanodot array (filled). (B) Cytochalasin D-treated (●) and untreated cells (▲) on 200-nm nanodot arrays were drawn to show the early onset of apoptosis triggered by cytochalasin D.

5 REFERENCES

[1] N. J. Sniadecki, R. A. Desai, S. A. Ruiz, C. S. Chen, Ann Biomed Eng. 34, 59,2006.
[2] M. Mrksich, Curr Opin Chem Biol. 6, 794, 2002.
[3] C. S. Chen, M. Mrksich, S. Huang, G. M. Whitesides, D. E. Ingber, Science. 276, 1425,1997.
[4] A. Curtis, C. Wilkinson, Biomaterials. 18, 1573, 1997.
[5] R. G. Flemming, C. J. Murphy, G. A. Abrams, S. L. Goodman, P. F. Nealey, Biomaterials. 20, 573, 1999.
[6] G. A. Abrams, S. L. Goodman, P. F. Nealey, M. Franco, C.J. Murphy, Cell Tissue Res. 299, 39, 2000.
[7] M. J. Dalby, M. O. Riehle, H. Johnstone, S. Affrossman, A. S. Curtis, Biomaterials. 23, 2945, 2002.
[8] C.-T. Wu, F.-H. Ko, H.-Y. Hwang, Microelectronic Engineering 83, 1567, 2006.
[9] M. A. Partridge, E. E. Marcantonio, Mol Biol Cell. 17, 4237, 2006.
[10] E. A. Clark, J. S. Brugge, Science. 268, 233, 1995.
[11] S. M. Frisch, H. Francis, J Cell Biol. 124, 619, 1994.
[12] R. O. Hynes, Cell. 69, 11, 1992.
[13] R. L. Juliano, S. Haskill, J Cell Biol. 120, 577, 1993.
[14] J. F. Casella, M. D. Flanagan, S. Lin, Nature. 293, 302, 1981.
[15] S. Celeste Morley, G. P. Sun, B. E. Bierer, J Cell Biochem. 88, 1066, 2003.
[16] R. Yao, G. M. Cooper, Science. 267, 2003, 1995.
[17] S. L. DeMeester, J. P. Cobb, R. S. Hotchkiss, D. F. Osborne, I. E. Karl, K. W. Tinsley, T. G. Buchman, Surgery. 124, 362, 1998.